



Detailed investigation of the surface mechanisms and their interplay with transport phenomena in alumina atomic layer deposition from TMA and water

Georgios Gakis, Hugues Vergnes, Emmanuel Scheid, Constantin Vahlas, Andreas Boudouvis, Brigitte Caussat

► To cite this version:

Georgios Gakis, Hugues Vergnes, Emmanuel Scheid, Constantin Vahlas, Andreas Boudouvis, et al.. Detailed investigation of the surface mechanisms and their interplay with transport phenomena in alumina atomic layer deposition from TMA and water. Chemical Engineering Science, 2019, 195, pp.399-412. 10.1016/j.ces.2018.09.037 . hal-02329135

HAL Id: hal-02329135

<https://hal.science/hal-02329135>

Submitted on 31 Aug 2023

HAL is a multi-disciplinary open access archive for the deposit and dissemination of scientific research documents, whether they are published or not. The documents may come from teaching and research institutions in France or abroad, or from public or private research centers.

L'archive ouverte pluridisciplinaire **HAL**, est destinée au dépôt et à la diffusion de documents scientifiques de niveau recherche, publiés ou non, émanant des établissements d'enseignement et de recherche français ou étrangers, des laboratoires publics ou privés.








Open Archive Toulouse Archive Ouverte (OATAO)

OATAO is an open access repository that collects the work of Toulouse researchers and makes it freely available over the web where possible

This is an author's version published in: <http://oatao.univ-toulouse.fr/21237>

Official URL: <https://doi.org/10.1016/j.ces.2018.09.037>

To cite this version:

Gakis, Giorgos  and Vergnes, Hugues  and Scheid, Emmanuel 
and Vahlas, Constantin  and Boudouvis, Andreas G. and Caussat,
Brigitte  *Detailed investigation of the surface mechanisms and
their interplay with transport phenomena in alumina atomic layer
deposition from TMA and water.* (2019) Chemical Engineering
Science. 195. 399-412. ISSN 0009-2509

Any correspondence concerning this service should be sent
to the repository administrator: tech-oatao@listes-diff.inp-toulouse.fr

Detailed investigation of the surface mechanisms and their interplay with transport phenomena in alumina atomic layer deposition from TMA and water

Georgios P. Gakis^{a,b}, Hugues Vergnes^b, Emmanuel Scheid^c, Constantin Vahlas^d, Andreas G. Boudouvis^{a,*}, Brigitte Caussat^b

^aNational Technical University of Athens, School of Chemical Engineering, Athens, Greece

^bLaboratoire de Génie Chimique, Université de Toulouse, Toulouse, France

^cLAAS, Université de Toulouse, Toulouse, France

^dCIRIMAT, Université de Toulouse, Toulouse, France

HIGHLIGHTS

- Surface mechanisms of alumina ALD are studied using a novel surface kinetic model.
- The GPC behavior within the ALD temperature window is investigated.
- Competition between desorption and reactions of adsorbed reactants is revealed.
- The effect of temperature on the surface kinetics is studied.
- The effect of transport phenomena on the uniformity of the film is revealed.

ARTICLE INFO

Keywords:

ALD
TMA
Surface mechanisms
CFD
Desorption
Alumina

ABSTRACT

The surface mechanisms involved in the Atomic Layer Deposition of Al_2O_3 from TMA and H_2O are investigated by means of combined experimental and computational analyses. Reactant adsorption, desorption and surface reaction are taken into account by a surface chemistry model, coupled to a CFD model for an industrial reactor treating 200 mm substrates. Once the model validated by comparison with experimental deposition rates, the relative contribution of each surface phenomenon is quantitatively determined between 100 and 300 °C through original reaction probability calculations. It is revealed that the competition between surface reactions and desorption of adsorbed H_2O plays a crucial role in the ALD growth of alumina. The H_2O desorption is the limiting factor for the growth at low process temperature whereas it is the OH group surface concentration at higher temperature. This integrated (surface chemistry/kinetics and CFD) model shows a direct link between transport phenomena, such as gas flow recirculation and low temperature zones in the reactor, and film uniformity.

1. Introduction

Atomic Layer Deposition (ALD) is a film deposition technique, based on the sequential exposure of a surface to gas phase reactants (Johnson et al., 2014). It is organized in reactant exposure steps, separated by a purging time period, during which the reactants are removed from the chamber, in order to avoid gas phase reactions among them (Johnson et al., 2014; Puurunen, 2005). Each

ALD system is referred to have a range of process temperature values ("ALD window") within which the deposition behavior is supposed ideal, and the growth per cycle remains constant (George, 2010).

The advantage of ALD relies on the self saturating chemisorption of the reactants on the surface, which ensures a high control over the thickness of the deposited film, and subsequently high uniformity and conformity under optimized conditions (George, 2010). This advantage allows ALD to meet the prerequisites for the production of new devices in numerous Key Enabling Technologies, which push towards smaller dimensions. Hence, the precise control of thickness in terms of growth and uniformity is

* Corresponding author.

E-mail address: boudouvi@chemeng.ntua.gr (A.G. Boudouvis).

Nomenclature

A_{des}	desorption pre exponential frequency factor, s^{-1}	k_{des}	desorption rate coefficient, s^{-1}
A_r	reaction pre exponential frequency factor of surface species k , s^{-1}	k_r	reaction rate coefficient, s^{-1}
C_i	molar concentration of gas phase species i , mol/m^3	M_i	molecular weight of gas phase species i , kg/mol
C_k	molar concentration of surface phase species k , mol/m^2	P	pressure, Pa
C_p	heat capacity of gas mixture, $J/(kg \cdot K)$	P_i	partial pressure of gas phase species i , Pa
C_{tot}	total concentration of surface species, mol/m^2	p_k	reaction probability of adsorbed species k
d	layer thickness, m	$p_{init,i}$	reaction probability of gas phase species i
D_{ik}	Maxwell Stefan Diffusion coefficient, m^2/s	Q	boundary heat flux, $J/(m^2 \cdot s)$
E_{ads}	adsorption activation energy, eV	R	ideal gas constant, $J/mol \cdot K$
E_{des}	desorption activation energy, eV	$R_{ads,i}$	adsorption rate of gas phase species i , $mol/(m^2 \cdot s)$
E_r	reaction activation energy, eV	$R_{des,k}$	desorption rate of adsorbed species k , $mol/(m^2 \cdot s)$
$Flux_i$	molar flux of gas phase species i , $mol/(m^2 \cdot s)$	$R_{r,k}$	reaction rate of adsorbed species k , $mol/(m^2 \cdot s)$
g	gravity acceleration, m/s^2	$S_{0,i}$	initial sticking probability of gas phase species i
H_i	enthalpy of formation of gas phase species i , J/mol	S_i	sticking probability of gas phase species i
h_{pl}	Planck constant, $J \cdot s$	T	temperature, K
I	unit tensor	u	velocity, m/s
J_i	boundary flux of gas phase species i , $kg/(m^2 \cdot s)$	x_i	molar fraction of gas phase species i
j_i	diffusive flux gas phase species i , $kg/(m^2 \cdot s)$	θ_k	surface coverage of surface species k
Kn	Knudsen number	μ	dynamic viscosity, Pa $\cdot s$
k_i	thermal conductivity of gas phase species i , $W/m \cdot K$	ρ	density, kg/m^3
k_b	Boltzmann constant, J/K	σ_k	site occupancy number of surface species k
		ω_i	mass fraction of gas phase species i

crucial, especially in the case of deposition on large area items. In turn, this level of control requires a deep understanding of the physicochemical mechanisms taking place on the surface during an ALD process, and of the effect of the process parameters, such as pressure and temperature, on those mechanisms.

One of the most studied ALD processes is the deposition of Al_2O_3 films, using tri methyl aluminum ($Al(CH_3)_3$, TMA) and H_2O vapor as metal precursor and oxidant source, respectively (Jur and Parsons, 2011; Wind and George, 2010; Dillon et al., 1995; Aria et al., 2016). A great number of works has been published on this chemical system (Groner et al., 2004; Ott et al., 1997; Elam et al., 2002) in numerous reactor configurations and a wide range of process conditions and substrates, establishing this system as a model one for the ALD process. However, certain aspects of the surface chemistry of this process are still not thoroughly understood. The limited growth under low process temperature has been the topic of recent research (Vandalon and Kessels, 2016, 2017). The growth dependence on the process temperature over the whole ALD temperature window indicates complex surface mechanisms. (Vandalon and Kessels, 2016, 2017). This dependence has not yet been explained in detail for the TMA + H_2O process. The competing physical and chemical mechanisms on the surface, such as the competition between desorption and surface reactions have not been studied, to the best of our knowledge.

In a theoretical perspective, physical based modelling has emerged as a powerful tool to study the fundamental reactions taking place during an ALD cycle. Theoretical studies can provide information that is difficult to access experimentally due to the very restricted length and time scales of the surface phenomena in ALD. Density functional theory (DFT) calculations (Murray and Elliott, 2013; Widjaja and Musgrave, 2002; Weckman and Laasonen, 2015; Delabie et al., 2012) are able to analyze the different reaction pathways that the reactants can undergo, concluding on the most favorable reactions, based on the activation energies needed to reach the transition state for each case. Using those energies, Travis and Adomaitis (2014, 2013) investigated the surface reaction kinetics and dynamics during the ALD cycle. Remmers et al. (2015) investigated the reaction dynamics using a reaction factorization study, while Holmqvist et al. (2014) esti-

mated the reaction kinetic parameters using a combined computational and experimental approach.

Computational Fluid Dynamics (CFD) models for ALD reactors have been developed to study the process at the reactor scale (Holmqvist et al., 2013). In a previous work, (Gakis et al., 2018) we showed that the reactor setup, geometry and process conditions can lead to undesirable flow regimes such as gas flow recirculation, and to non uniform temperature fields. Xie et al. (2015) combined a detailed surface chemistry model with a reactor CFD model in order to study the effect of temperature and pressure on the deposition process. Holmqvist et al. published a series of articles (Holmqvist et al., 2012, 2013a, 2013b, 2014), using a continuous flow reactor model to investigate the reactant flow, allowing the mechanistic analysis of the ALD reactions. Using this model, the reactor scale up and process optimization were studied. Pan et al. (2015) studied the effect of the position of the sample inside the reactor, while Peltonen et al. (2018) studied the flow during ALD process, correlating the film uniformity with fluid dynamical aspects. Shaeri et al. (2014) studied the effect of reactor design on the reaction rates and the uniformity of the deposition rate at certain snapshots during alumina ALD. However, the latter analysis was not validated by experimental measurements, and no investigation on the final thickness uniformity was performed. It is crucial that the effect of the process parameters in an industrial reactor with a complex design, on film characteristics such as film uniformity, be thoroughly studied. Such analyses will help obtain a road map towards reactor design and process optimization, to achieve the production of uniform films.

This work aims the detailed investigation of the surface mechanisms that affect the film deposition inside the temperature window of alumina ALD. It is the first time that the competition between desorption and reaction of the adsorbed reactant species is discussed in detail for the TMA + H_2O process. In this work, this competition and its effect as a limiting factor for the ALD growth is revealed using a computational approach, validated by experimental measurements. The effect of the reactive sites present on the substrate is analysed as well. Our previously presented three dimensional CFD model for a commercial ALD reactor, (Gakis et al., 2018) is coupled to an original surface kinetics model, incor-

porating reactant adsorption, desorption, and surface reaction. The simulation results for the growth per cycle and thickness uniformity obtained are validated by comparison with experimental ones at the surface and reactor scales. Furthermore, we apply this model to reveal and investigate the effect of the reactor design and transport phenomena inside the ALD reactor chamber onto the deposited film thickness and uniformity. A direct link between complex transport phenomena, reactor design and process parameters resulting from the reactor and process setup and film uniformity is presented.

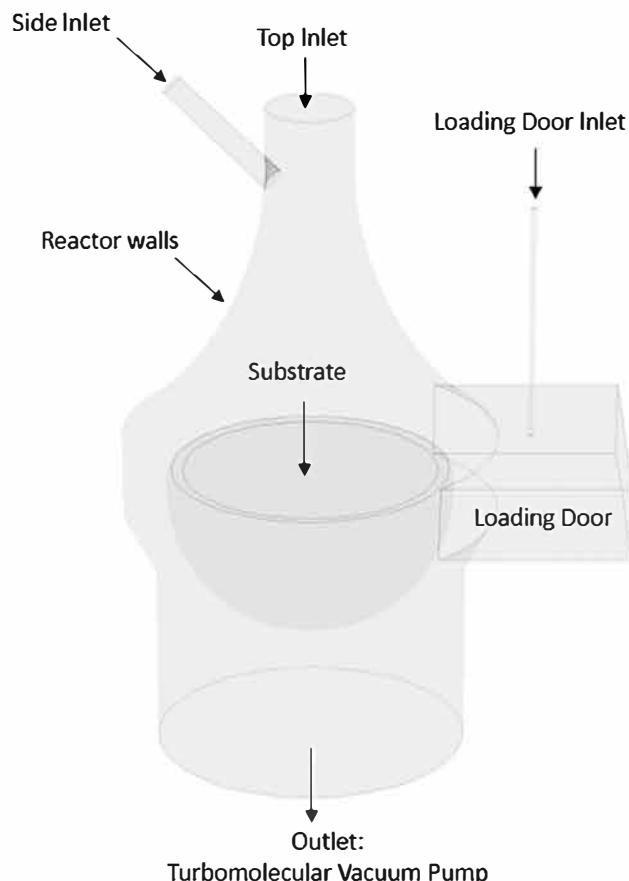


Fig. 1. Schematics of the Ultratech® Fiji F200 ALD reactor chamber.

2. Materials and methods

The Al_2O_3 films were deposited using a commercial Ultratech® Fiji F200 ALD setup. The schematics of the ALD reactor chamber is presented in Fig. 1.

An extensive description of the ALD system setup has been presented in our previous work (Gakis et al., 2018). In this section a brief description is provided. The reactor has three gas inlets, here after called top inlet, side inlet, and loading door inlet, as shown in Fig. 1. A steady flow of argon (Ar) is permanently fed to the reactor via all the inlets. The Ar flow through all inlets is regulated by mass flow controllers (MFC), while the reactant pulses are controlled by the opening time of ALD valves in the feeding system, connected to the side inlet of the reactor (Gakis et al., 2018). Pumping is ensured by a turbo molecular pump and the pumping speed and base pressure are regulated with an automatic pressure controller (APC) unit. The reactor walls and the precursor feeding system are heated via a jacket, while the substrate is heated via a chuck. The loading door walls are not heated.

TMA and H_2O vapor were used as metal precursor and oxidant source, respectively. The alumina films were deposited on 200 mm diameter Si (100) wafers. The wafers were pretreated by deionized (DI) water rinsing, followed by dipping in a 5% HF solution for 1 min, in order to remove the native oxide on the Si surface, and a final DI water rinsing. After the pretreatment, the wafer was dried and immediately loaded into the chamber, which was pumped out to its base pressure (10^{-4} – 10^{-5} Torr) during 10 min, then to the pressure of the ALD process (72 mTorr) during 5 min. The pulsing and purging times being set, the isolation valve of the capacitance manometer was closed and the process was initiated. The cycles were repeated until a certain number of cycles, corresponding to the desired thickness, was attained.

Deposition takes place under process conditions that are implemented according to predefined recipes. In all experiments, the top inlet, loading door and side inlet Ar flows were set to 100 sccm, 50 sccm and 30 sccm, respectively. The top and loading door gas temperatures were set at 20 °C and the side inlet gas temperature at 150 °C. The opening of the ALD valve for the H_2O exposure was set to 0.1 s. The adopted experimental conditions for fifteen ALD experiments are shown in Table 1.

The thickness of the deposited films was measured via ellipsometry with a Horiba UVISSEL Variable Angle Spectroscopic Ellipsometer. The wavelength interval ranged between 265 and 650 nm. We chose to deposit films with quite high thickness (50–60 nm). So as to minimize the measurement error due to any uncertainty on the thickness and composition of the interface between the silicon substrate and the pure Al_2O_3 deposited film,

Table 1
Thermal and cycle conditions used for the ALD reactor.

Experiment #	Substrate center temperature (°C)	Reactor walls temperature (°C)	TMA pulse time (s)	TMA purge time (s)	H_2O purge time (s)	Number of cycles
1	125	125	0.025	30	30	500
2	125	125	0.060	30	30	500
3	150	150	0.025	20	20	500
4	150	150	0.060	20	20	500
5	162	162	0.025	20	20	500
6	175	175	0.025	15	15	500
7	175	175	0.060	15	15	500
8	200	200	0.025	10	10	500
9	200	200	0.060	10	10	500
10	250	250	0.060	8	8	500
11	300	270	0.025	5	5	550
12	300	270	0.060	5	5	550
13	300	270	0.025	2	3	550
14	150	150	0.025	10	10	500
15	150	150	0.060	5	5	500

3. Computational model formulation

3.1. Reactor CFD model

The governing equations that describe the transport phenomena taking place inside the ALD reactor include the conservation of mass, momentum, and energy, coupled with the conservation of chemical species, as detailed in supplementary material. The maximum Knudsen number calculated during the argon purge step was lower than 7×10^{-3} , taking the outlet diameter as a characteristic length, thus validating the continuous regime assumption. The thermal conductivity, dynamic viscosity, and diffusion coefficients for the chemical species are computed using the kinetic gas theory. The Lennard Jones parameters for the species are obtained from the CHEMKIN PRO database (CHEMKIN PRO, 2013). The gas is considered as ideal. The gas is also considered as a Newtonian fluid and the flow is laminar.

The maximum Reynolds number was calculated at 300 °C. During the purging times, the Reynolds number was found 2.05, while the maximum value during the reactant pulses was 129.15 for the TMA pulse and 37.08 for the H₂O pulse, at the side inlet. The characteristic length used was the side inlet diameter, as this was the region where the maximum was found.

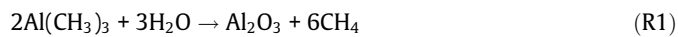
The above equations are discretized and solved using Comsol Multiphysics®, which uses the finite element method. The computational mesh used for the spatial discretization of the computational domains was also generated by Comsol Multiphysics. A quadratic basis functions set was selected for approximating the velocity and the species mass fractions, while a linear basis functions set was used for temperature and pressure.

The computational mesh consists of 149 226 tetrahedral elements, while the dimensionless wall distance of the first element height in the normal direction to the substrate is 0.01732, using the substrate diameter as a characteristic length.

No slip boundary conditions is implemented on the reactor walls, while a flow rate equal to the Argon inlet flow rates described in Section 2 is imposed as inlet boundary condition during the purge times. A steady volumetric flow rate equal to 57.12 L/s is imposed at the outlet, in order to simulate the turbo molecular vacuum pump. For more information regarding the outlet pump simulation, as well as for the inlet conditions during the reactant pulses and the substrate thermal boundary conditions, the reader is referred to our previous work (Gakis et al., 2018). A zero species flux condition is imposed on the reactor walls, while the wall temperatures are set to the values of Table 1, to simulate the respective experiment. The reactor model is coupled to the surface chemistry model through the substrate boundary conditions, which are presented below, in Section 3.4.

3.2. Surface chemistry

The overall reactions taking place during the ALD cycle are the following:



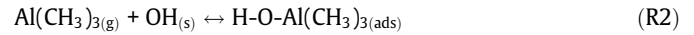
The thermodynamic properties of the reactants are ideal, as they are volatile at room temperature, and TMA is not decomposing up to 300 °C (Puurunen, 2005).

In this section the possible chemical mechanisms taking place during the ALD process are presented. For more clarity, we detail separately the phenomena occurring at each reactant exposure.

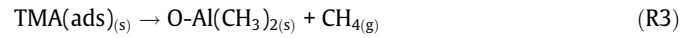
3.2.1. TMA exposure

The adsorption and reaction of TMA molecules during the ALD regime take place on hydroxyl groups, which serve as reactive

sites. The first mechanism taking place during the TMA exposure is the reversible adsorption of TMA on a surface hydroxyl group:

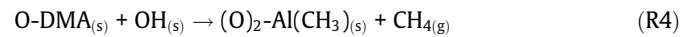


hereafter named TMA(ads)_(s). This TMA molecule, after it adsorbs on the OH site, can either desorb or proceed in a reaction where a CH₃ ligand of TMA reacts with the hydrogen atom of the hydroxyl group, forming CH₄ that is desorbed as a gaseous byproduct:



where the Al(CH₃)₂(s) surface species is hereafter referred to as Dimethyl aluminum or DMA.

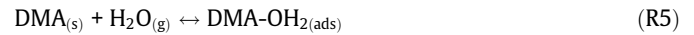
Studies using density functional theory calculations (Weckman and Laasonen, 2015) showed that a DMA molecule can undergo a second reaction with a neighbouring OH site on the surface, releasing CH₄ as a gaseous by product and forming an aluminum bridge between the neighbouring O sites:



with the new Al(CH₃)_(s) surface species hereafter referred to as monomethyl aluminum, or MMA.

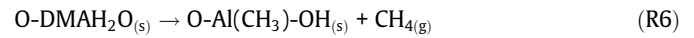
3.2.2. Water exposure

During the water pulse, the methyl terminated surface generated by the previous TMA step of the cycle, is exposed to H₂O vapor. The H₂O molecules adsorb on the DMA species:



onwards called DMAH₂O_(s).

The adsorbed H₂O molecule can then either desorb or react with one of the methyl groups, leaving a OH group at its place, and releasing CH₄ as a byproduct:

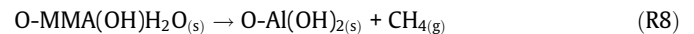


with the Al(CH₃) OH_(s) species hereafter named MMAOH_(s).

A second H₂O molecule then adsorbs on the MMAOH species:



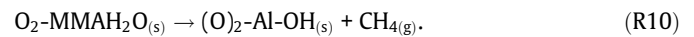
onwards called MMA(OH)H₂O_(s), which can then either desorb or react with the methyl group on the surface, releasing CH₄, leaving the surface OH terminated:



Finally, water can adsorb on MMA species on the surface:



onwards called MMAH₂O_(s), which can either desorb or react with the methyl group on the surface, releasing CH₄ and leaving the surface OH terminated:

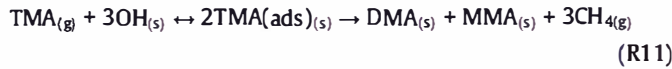


3.3. Implementation of the surface chemistry

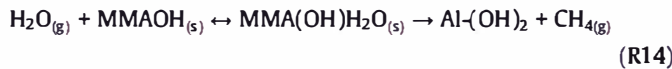
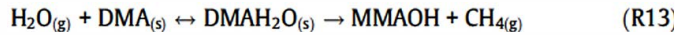
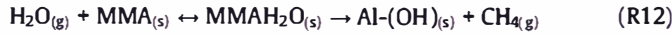
In this section, we present the selected mechanisms implemented in the surface chemistry model. We model the growth of the deposited film within the ALD regime, where the growth per cycle (GPC) is constant as a function of the number of cycles. Therefore, after each ALD cycle, the surface must be regenerated so as to maintain a constant number of OH groups on the surface from one cycle to another, while depositing stoichiometric alumina. As previously described, the initial reaction of a TMA molecule with a hydroxyl group on the surface may be followed by a further reaction with a neighbouring hydroxyl. Taking into account the mechanisms in the previous section, the surface after the TMA pulse

must contain equal proportions of MMA and DMA species. This ensures the stoichiometric overall reaction, where two TMA molecules react with three H₂O molecules, producing Al₂O₃. Therefore, we implement this condition to our mechanism, leading to the following overall reactions at each reactant exposure.

For the TMA exposure:



For the H₂O exposure:



The reaction mechanism is schematically presented in Fig. 2.

The model takes into account gas molecule adsorption (reactions R2, R5, R7, R9), desorption of adsorbed molecules (reverse reactions R2, R5, R7, R9) and forward surface reactions of the adsorbed molecules. The adsorption rate of each adsorption step for species *i* ($R_{ads,i}$) is given by the following equation, in mol m⁻² s⁻¹:

$$R_{ads,i} = s_i \cdot \text{Flux}_i \quad (1)$$

where Flux_i is the molar flux of gaseous species *i*, and *s* is the sticking coefficient.

The molar flux is computed by the Hertz Knudsen equation:

$$\text{Flux}_i = \frac{P_i}{\sqrt{2\pi M_i RT}} \quad (2)$$

where P_i is the species *i* partial pressure, M_i is its molecular mass, R is the ideal gas constant, and T is the temperature. The sticking coefficient depends on the surface coverage of surface sites which are available for the species *i* to deposit on. The surface coverage of each surface species *k* is denoted as θ_k , and the sum of all coverages of the surface sites, *n* in number, must be equal to unity.

$$s_i = s_{0,i} \cdot \theta_{av} \cdot e^{\frac{E_{ads}}{k_b T}} \quad s_{0,i} \cdot (1 - \theta_{nomv}) \cdot e^{\frac{E_{ads}}{k_b T}} \quad (3)$$

$$\sum_{k=1}^n \theta_k = 1 \quad (4)$$

In Eq. (3), E_{ads} is the activation energy for adsorption, k_b is the Boltzmann constant, T is the temperature, $s_{0,i}$ is the initial sticking probability of species *i*, when the whole surface is available for deposition, and no energy barrier needs to be overcome i.e. $\theta_{av} = 1$. The $s_{0,i}$ value is treated as a model parameter. The surface coverage of each species is given by:

$$\theta_k = \sigma_k \frac{C_k}{C_{tot}} \quad (5)$$

where σ_k is the site occupancy number, C_k and C_{tot} are the surface concentration of species *k* and the total concentration of surface sites, respectively, both in mol m⁻². The site occupancy number describes how many surface sites are occupied by each surface

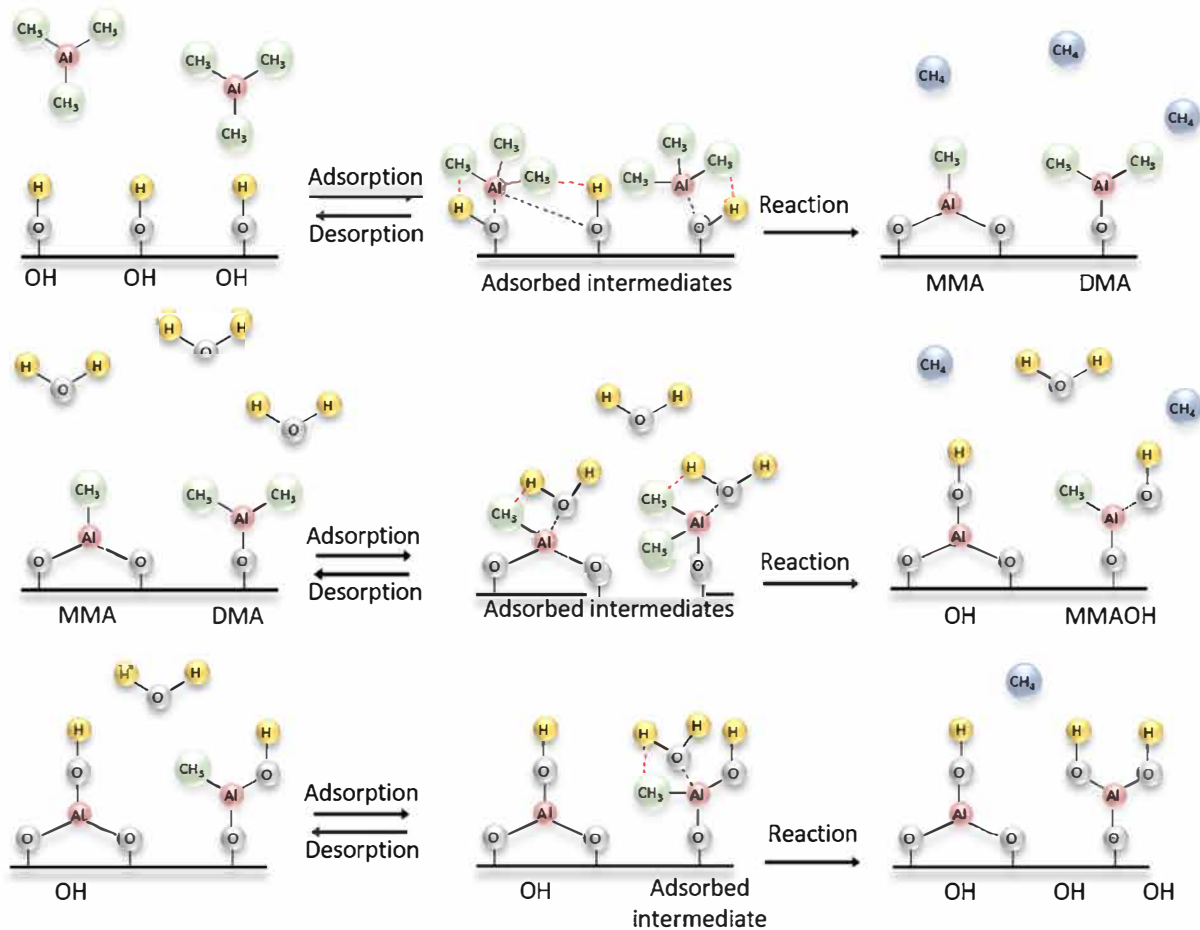


Fig. 2. Schematics of the chemical mechanism implemented in the surface chemistry model.

species. In our case, C_{tot} is the maximum number of OH groups that can be present on the surface, which depends on the surface temperature.

The reversible step of adsorption, i.e. the desorption of the adsorbed surface species k on the surface is modelled as a first order surface reaction:

$$R_{\text{des},k} = k_{\text{des},k} \cdot C_k \quad (6)$$

where R_{des} is the desorption rate of adsorbed surface species k , in $\text{mol m}^{-2} \text{s}^{-1}$, and $k_{\text{des},k}$ is the desorption rate coefficient in s^{-1} , that is computed using an Arrhenius expression:

$$k_{\text{des},k} = A_{\text{des},k} \cdot e^{-\frac{E_{\text{des},k}}{k_b T}} \quad (7)$$

where $A_{\text{des},k}$ is the pre exponential frequency factor, E_{des} is the activation energy for the desorption of a molecule, and k_b is the Boltzmann constant.

The surface reactions are treated the same way as desorption:

$$R_{r,k} = k_{r,k} \cdot C_k \quad (8)$$

$$k_{r,k} = A_{r,k} \cdot e^{-\frac{E_{r,k}}{k_b T}} \quad (9)$$

By developing the mechanism described above using the described phenomena, we have 8 surface species, namely $\text{OH}_{(s)}$, $\text{TMA(ads)}_{(s)}$, $\text{DMA}_{(s)}$, $\text{MMA}_{(s)}$, $\text{DMAH}_2\text{O}_{(s)}$, $\text{MMAOH}_{(s)}$, $\text{MMA(OH)}_{(s)}$, $\text{H}_2\text{O}_{(s)}$, $\text{MMAH}_2\text{O}_{(s)}$. The surface species conservation equations are treated during each pulse, and are presented in the supplementary material.

3.4. Coupling of the CFD and surface chemistry models

The coupling the CFD model with the surface chemistry one is realized through the boundary conditions implemented on the substrate surface, for the species transport and heat transport equations. On the substrate surface, a species flux is implemented as a boundary condition for TMA, H_2O , and CH_4 species.

$$J_{\text{TMA}} = (R_{\text{ads},\text{TMA}} - R_{\text{des},\text{TMA(ads)}}) \cdot M_{\text{TMA}} \quad (10)$$

$$J_{\text{H}_2\text{O}} = -\left(R_{\text{ads},\text{DMAH}_2\text{O}} + R_{\text{ads},\text{MMA(OH)H}_2\text{O}} + R_{\text{ads},\text{MMAH}_2\text{O}} - R_{\text{des},\text{DMAH}_2\text{O}} - R_{\text{des},\text{MMA(OH)H}_2\text{O}} - R_{\text{des},\text{MMAH}_2\text{O}}\right) \cdot M_{\text{H}_2\text{O}} \quad (11)$$

$$J_{\text{CH}_4} = (1.5 \cdot R_{r,\text{TMA(ads)}} + R_{r,\text{MMAH}_2\text{O}} + R_{r,\text{DMAH}_2\text{O}} + R_{r,\text{MMA(OH)H}_2\text{O}}) \cdot M_{\text{CH}_4} \quad (12)$$

where J (in $\text{kg/m}^2 \text{s}$) is the species mass flux, with the positive sign denoting that the species is generated at the surface.

A heat flux is also generated on the substrate surface, corresponding to the enthalpies of the surface reactions:

$\dot{Q} = \sum_{m=1}^r R_m \cdot \Delta H_m$, where r is the total number of reactions, and ΔH is the reaction enthalpy.

3.5. Computational parameters

The most significant difficulty in modelling this process is the absence of data regarding the reactant pulses that are injected into the ALD reactor during the exposure steps of the cycle, as no measuring device is installed. In order to simulate the ALD process however, the reactant pulses must be known. This is the reason why a CFD model for the reactant feeding system was built, described in our previous work (Gakis et al., 2018). In order to couple the two models, that is the CFD model for the reactor and the CFD model for the feeding system, a specific scheme, presented in Gakis et al. (2018) was used.

For the surface chemistry model, values regarding the activation energies, reaction enthalpies, sticking coefficients, initial maximum concentration of surface sites and pre exponential factors must be set. The activation energies and reaction enthalpies are taken from Widjaja and Musgrave (2002), where are reported the computed energy barriers needed for the adsorbed TMA molecule to react according to (R3). These energy barriers are used as activation energies for the TMA surface reactions. In these studies, the adsorption step of the gaseous TMA molecule on a OH site is exothermic. This binding energy of the TMA is used in our study as the activation energy for desorption. The same is done for the water activation energies for surface reaction and desorption on DMA and MMAOH sites. We assume that the energies for the H_2O reaction and desorption on the MMA species are equal to those on DMA, calculated by Widjaja and Musgrave (2002).

The initial surface is assumed to be covered by OH sites, i.e. $C_{\text{init, OH}} = C_{\text{tot}}$. The value of C_{tot} hence indicates the maximum number of OH groups that can be present on the surface. As the deposition of Al_2O_3 is dependent on the surface OH (Puurunen, 2005) site concentration, this maximum concentration must be carefully chosen. The maximum OH concentration depends on the temperature, as the OH groups are thermally unstable. Two neighbouring OH sites can react with each other, in order to form an oxygen bridge and desorb one molecule of H_2O (Puurunen, 2005; Zhuravlev, 2000). In our study, the maximum OH concentration is implemented as a function of the surface temperature, based on data on silica surface reported by Haukka and Root (1994). This data shows an almost linear relation between the OH concentration and the silica surface temperature, for the range of 200–560 °C. This behavior has also been reported in Dillon et al. (1995) on porous alumina. We assume that the same relation is also valid at lower temperatures down to 125 °C, and we implement this linear relation to calculate the maximum OH concentration for each process temperature.

The pre exponential factors were assumed to be equal to:

$$A = \frac{k_b T}{h_{\text{pl}}} \quad (13)$$

for all surface reactions and desorption, where k_b is the Boltzmann constant, T is the temperature, and h_{pl} is the Planck constant. With the above model assumptions and parameters, only the initial sticking coefficients need to be determined.

In our study, the sticking coefficient of H_2O was assumed to be equal on all three available sites (DMA, MMA, MMAOH). Hence the surface chemistry model has two fitting parameters ($S_{0,\text{TMA}}$, $S_{0,\text{H}_2\text{O}}$).

The parameters used for our chemistry model are summarized in Table 2.

A discussion regarding the choice of the activation energies from the literature, as well as a sensitivity analysis of the model to those values, is presented in the supplementary material of the present work.

4. Results and discussion

4.1. Surface chemistry model

4.1.1. Effect of temperature on the film growth per cycle

In order to analyze the kinetics of the surface reactions, a study of the growth of the film as a function of temperature is performed, both computationally and experimentally, for two different TMA pulse durations. As we assume an ideal ALD regime, the thickness of the deposited film is divided by the respective number of ALD cycles used, in order to determine the growth per cycle (GPC). As the fully hydroxylated surface is used as an initial surface condition, the GPC obtained by the chemistry model is not constant from the first cycle onwards. A certain number of cycles need to be

Table 2
Computational parameters for the surface chemistry model.

Parameter	Value
Adsorption activation energy (Widjaja and Musgrave, 2002)	TMA: 0, H ₂ O: 0
Desorption activation energy (Widjaja and Musgrave, 2002)	TMA: 0.61 eV, H ₂ O on DMA and MMA: 0.57 eV, H ₂ O on MMAOH: 0.74 eV
Reaction activation energy (Widjaja and Musgrave, 2002)	TMA: 0.52 eV, H ₂ O on DMA and MMA: 0.7 eV, H ₂ O on MMAOH: 0.91 eV
Reaction Enthalpy (Widjaja and Musgrave, 2002)	TMA: 1.09 eV, H ₂ O on DMA and MMA: 0.91 eV, H ₂ O on MMAOH: 0.56 eV
Maximum OH concentration (Haukka and Root, 1994)	$y = -2.1661E-08 \cdot T + 1.68935E-05$, in mol/m ² , Derived from (Haukka and Root, 1994)
Sticking coefficient	$s_{0,TMA} = 0.004$ (Fitted), $s_{0,H_2O} = 0.014$ (Fitted)

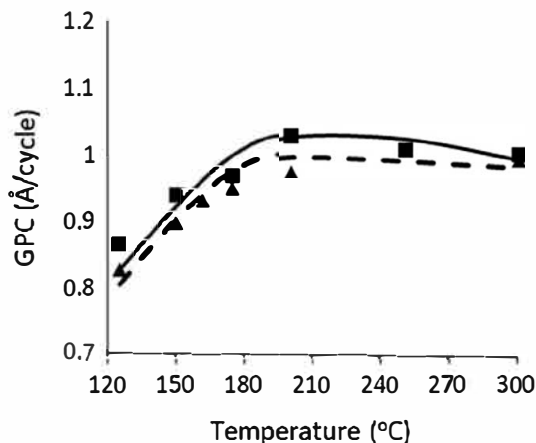


Fig. 3. GPC as a function of temperature. 25 ms TMA pulse: Triangles (experiments), dashed line (model). 60 ms TMA pulse: Squares (experiments), bold line (model).

simulated first, so that the kinetics implemented in the model lead to a constant GPC as it will be detailed in Section 4.3.

The thickness of the layer was calculated using the following equation:

$$h = \frac{M_{Al_2O_3}}{\rho_{Al_2O_3}} \frac{C_{Al_2O_3}}{\rho_{Al_2O_3}} \quad (14)$$

where $M_{Al_2O_3}$ is the molecular mass of alumina, $C_{Al_2O_3}$ is the bulk concentration of the produced alumina film, and $\rho_{Al_2O_3}$ is the density of alumina, taken at 3500 kg/m³ (Ott et al., 1997).

The comparison of the experimental (experiments 1–12 in Table 1) and calculated GPC at the center of the substrate (Simulated experiments 1–12), as a function of temperature and the TMA pulse duration, is presented in Fig. 3.

The model accurately predicts the experimental GPC for this range of operating conditions. Therefore, the model will be used for the analysis of the surface chemistry mechanism.

When using a 25 ms TMA pulse, for the range of 125–300 °C, the measured GPC increases with temperature from $0.83 \frac{\text{\AA}}{\text{cycle}}$ at 125 °C (experiment 1) to $1.03 \frac{\text{\AA}}{\text{cycle}}$ at 300 °C (experiment 11). This can be explained by the thermal activation of surface reactions, which under low temperatures will not occur or will be too slow. When a 60 ms TMA pulse is used, an overall increase of the GPC is both measured and computed in comparison with 25 ms. This implies that the TMA pulse of 25 ms was not long enough to cover the whole surface.

For the experiments with 60 ms TMA pulse, the GPC increases with temperature in the range 125–200 °C, as in the case of the 25 ms TMA pulse, this time reaching $1.03 \frac{\text{\AA}}{\text{cycle}}$. Further temperature increase leads to a slight GPC decrease, with the value of the GPC at 300 °C being $1.0 \frac{\text{\AA}}{\text{cycle}}$. This behavior has been reported in other works (Ott et al., 1997; Vandalon and Kessels, 2016; Pan et al., 2015; Xie

et al., 2015). It is usually ascribed to the activation of the TMA desorption at high temperature.

In our experiments, the GPC value at 300 °C (experiments 11 and 12) changes slightly with the increase of the TMA pulse; at 300 °C the OH surface sites were almost totally covered even with the 25 ms TMA pulse.

The surface chemistry model takes into account species adsorption, desorption, and surface reaction, as well as the surface OH concentration as a function of process temperature. The experimental behavior reveals a complex mechanism and the surface chemistry model with all the considered phenomena seems capable to catch this complexity, thus validating our analysis in the considered parametric window.

4.1.2. Reaction mechanisms

Before discussing the results of the surface chemistry model, the activation energies associated with each mechanism can give useful insight. Results from Widjaja and Musgrave (2002) summarized in Table 2, show that the adsorption step has no activation energy barrier for TMA nor H₂O. Hence, as we assume a steady initial sticking coefficient s_0 for each species as a function of temperature, the adsorption step, at each time, will depend on the species flux on the surface and the state of the surface. The adsorbed reactant molecule can then either react on the surface, with an irreversible reaction, or desorb. These are two competing mechanisms, taking place at the same time on the surface, and their relative rates will show whether the reaction or the desorption is more favorable. This competition has not been thoroughly discussed in previous works.

Again, results from Widjaja and Musgrave (2002) presented in Table 2, show that for the adsorbed TMA molecule, the activation energy for desorption is higher than the energy barrier to reach its transition state, from which the irreversible reaction step is exothermic. Therefore, the adsorbed TMA molecule is more likely to react on the surface, producing DMA and subsequently MMA species, than desorbing back to the gas phase. The opposite is shown for H₂O. The adsorbed H₂O molecule desorption has a lower energy barrier than the irreversible surface reaction, meaning that the adsorbed H₂O molecule is more likely to desorb than react on the surface.

To study these behaviors as a function of temperature, we introduce a reaction probability approach. Specifically, we study the reaction probability, p_k , of an already adsorbed molecule k , given as the ratio of the forward surface reaction rate R_r to the sum of the rates of the possible events, i.e. reaction and desorption rates.

$$p_k = \frac{R_r}{R_r + R_d} \quad (15)$$

Here k denotes that the adsorbed molecules are surface species. If we multiply this value with the initial sticking coefficient $s_{0,i}$ for each gas species, we obtain the total initial probability p_i of a gas molecule i to adsorb and react on the surface, fully covered by available adsorption sites.

$$D_{init,i} = s_{0,i} \cdot p_i \quad (16)$$

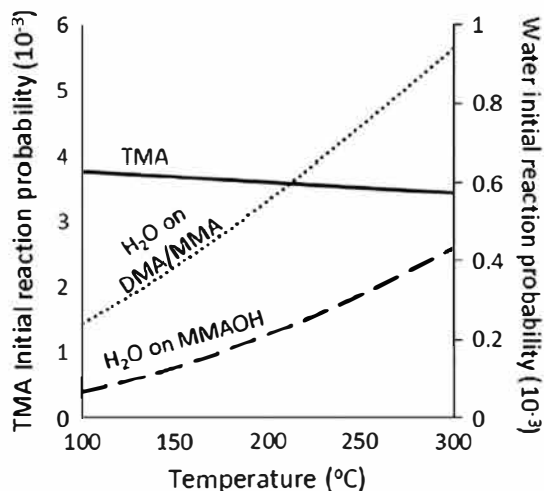


Fig. 4. Model predictions for the gas species initial reaction probabilities $p_{init,i}$: TMA (continuous line, left hand axis), H₂O on DMA/MMA species (dotted line, right hand axis) and H₂O on MMAOH species (dashed line, right hand axis).

Here, i denotes gas phase species. The dependence of the initial reaction probability of the gas species is shown in Fig. 4.

At 100 °C, the reaction probability of a TMA molecule is $p_{init,TMA} = 3.77 \cdot 10^{-3}$, a low value due to the low sticking probability ($s_{0,TMA} = 0.004$). Once the TMA molecule is adsorbed, it has a $p_{TMA} = 94\%$ probability of reacting (Eq. (15)). As the temperature increases, the TMA desorption is activated, and the reaction probability slightly decreases. At 300 °C, the reaction probability of the adsorbed TMA is $p_{TMA} = 86\%$, while the overall initial probability is $p_{init,TMA} = 3.44 \cdot 10^{-3}$. It is seen that the reaction probability of the already adsorbed TMA on the surface is high for all temperatures. Hence, the TMA step is limited by the adsorption process, and the low sticking probability of the molecule. To obtain a maximum coverage of the surface after the TMA pulse, the pulse duration must be adjusted, so that the TMA chemisorbs on the whole substrate surface. The temperature has a small effect on the reaction probability of TMA. The results for the TMA initial reaction probability are in good agreement with those experimentally found by Vandalon and Kessels (2016) and confirm the small effect of temperature on the TMA half step discussed in this work.

Fig. 4 also shows the reaction probabilities of H₂O molecules on the adsorbed DMA, MMA and MMAOH species. It is shown that for 100 °C, the reaction probability of H₂O is $2.4 \cdot 10^{-4}$ on DMA and MMA, while a lower value of $0.7 \cdot 10^{-4}$ is computed on MMAOH. These low probabilities are due to the higher activation energy for the surface reaction than for desorption. In addition to the higher activation energies of the H₂O reactions, growth at low process temperatures is also impacted by the lower energy barrier for desorption of the H₂O molecule, leading to incomplete H₂O reactions.

As temperature increases, both surface reaction and desorption are activated, with the latter at a smaller rate. The resulting reaction probability increases, reaching $9.3 \cdot 10^{-4}$ on DMA and MMA, and $4.3 \cdot 10^{-4}$ on MMAOH at 300 °C. Based on these values, our model shows that the limiting mechanism would be the removal of the methyl group present on the MMAOH species. This could possibly be related to the conclusions of Vandalon and Kessels (2016, 2017) namely that isolated CH₃ groups are persistent and harder to remove during the H₂O exposure.

The probability of already adsorbed H₂O molecules to react are computed to be $p_{H_2O} = 1.72\%$ on DMA and MMA, and $p_{H_2O} = 0.5\%$ on MMAOH at 100 °C. With the increase of temperature, these values reach $p_{H_2O} = 6.7\%$ on DMA and MMA and $p_{H_2O} = 3.1\%$ on MMAOH at

300 °C. The sticking probability for the H₂O molecules ($s_{0,H_2O} = 0.014$) is higher than the TMA sticking probability ($s_{0,TMA} = 0.004$) thus showing that the adsorption step is faster for H₂O. However, the competition with desorption is very significant in the H₂O case, leading to less than 7% of adsorbed H₂O molecules to react on DMA, MMA and MMAOH species, even at 300 °C. These values are significantly lower than for the TMA molecules, explaining the longer exposure times needed for the H₂O step, and the effect of temperature on the activation H₂O reactions (Vandalon and Kessels, 2016, 2017).

The values predicted for the initial reaction probabilities of H₂O on MMAOH are close to the ones in literature taking into account the uncertainty of the measurements and calculations for the reactant flux reported by Vandalon and Kessels (2016).

It can then be deduced from these results that the GPC increase with temperature in the region 125–300 °C is attributed to the H₂O half reactions, and their competition with desorption. An increase of temperature favors the H₂O reactions with the methyl groups on the surface, hence leading to a higher GPC. The decrease of the GPC at higher temperatures can be attributed to two factors. Both the TMA desorption is favored and the maximum OH groups concentration on the surface decreases with temperature. However, as Fig. 4 shows, the relative decrease of the TMA probability with temperature is not very significant. The decrease of the GPC is thus attributed to the maximum number of OH groups. This will be further discussed in the next section.

4.1.3. Surface coverage dynamics

Fig. 5 presents the evolution of the surface coverage of all stable (OH, DMA, MMA and MMAOH) species, as a function of the number of cycles at 150 °C and 25 ms of TMA pulse (simulated experiment 3 of Table 1), at the center of the wafer for the five first simulated cycles. For the sake of clarity, the purge time is omitted. The exposure step of each reactant is shown as a half cycle, and each half cycle duration corresponds to 1.2 s. This time duration has been chosen as after that time, the reactant flux on the substrate surface is not significant enough to impact the adsorption reaction process.

Results show that, starting from a fully hydroxylated surface, the surface coverage of all four surface species reaches a steady regime after a certain number of cycles. In this regime, the surface state at the end of each cycle is the same as at its start, and the GPC is constant. Characterizations (not shown here, to be published in a forthcoming work) showed no carbon contamination. In the simulation, all methyl intermediate species formed during the cycle, in particular MMAOH, are eliminated during the next cycle and immediately re formed in the same proportions on the new reactive surface, so as to have no buried carbon.

In Fig. 5, the OH surface species start from a surface coverage of 1 in the first cycle, while in the steady regime (cycles 4 and 5) the surface coverage of OH groups at the start and end of the ALD cycle is 0.685. The same trend is observed for the coverage of the DMA and MMA species, at the end of the TMA pulse. The MMAOH groups are the most difficult to remove. Hence, during the 3 first cycles of deposition, the MMAOH coverage of the surface increases after each cycle. Once the steady regime is established (4th and 5th cycles), the MMAOH serves as an intermediate species, generated from the hydroxylation of a DMA and removed by the second hydroxylation of its last methyl group. This explains why the MMAOH coverage on the surface at the start and end of each cycle in the steady regime remains constant, as for all the other species.

The above observations confirm that the major mechanisms limiting the ALD growth at low temperature such as 150 °C are the H₂O reactions. However, as shown experimentally and predicted by the model, an increase to the TMA pulse duration

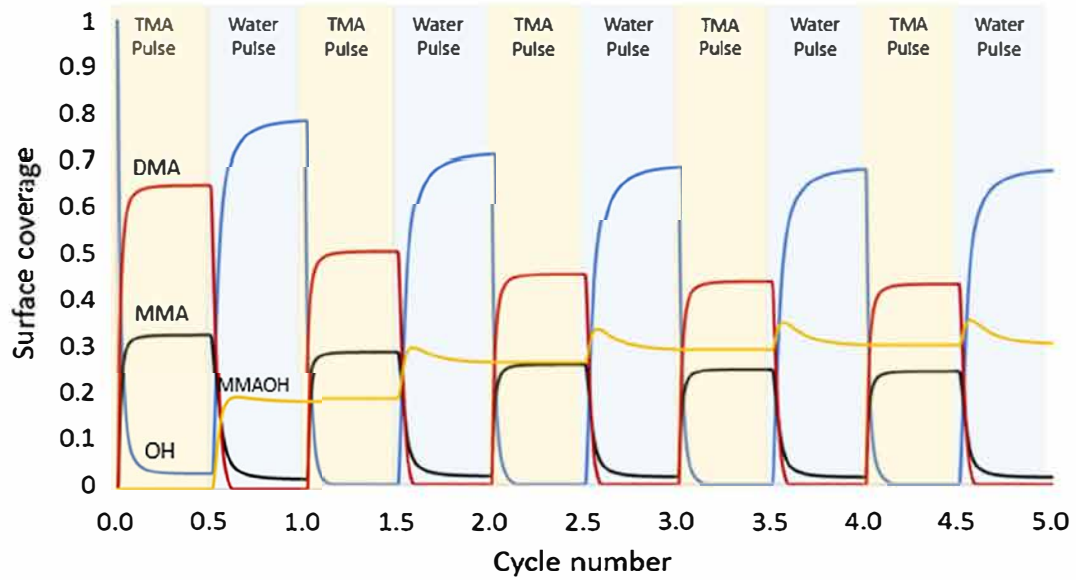


Fig. 5. Model predictions of the surface coverage evolution of the four stable surface species during the 5 first simulated cycles in simulated experiment 3.

increases the GPC (Fig. 3). Indeed, both the TMA and H₂O pulses inhibit the growth, when using a 25 ms TMA pulse. However, the H₂O step is the thermally activated mechanism, as discussed in the previous section. The H₂O reaction with MMAOH is the main mechanism limiting the growth at low temperatures. This is why the increase of the TMA pulse duration leads only to a marginal increase of the GPC. This is consistent with results of [Vandalon and Kessels \(2016\)](#) who showed that at low temperature, the growth of the alumina thermal ALD process is limited by the H₂O step, which is unable to remove persistent methyl groups on the surface.

When the steady regime is reached, all surface species concentrations present the same evolution; they are generated and

eliminated, and their coverage at the start of each cycle is the same. This regime is dependent on the surface reactions, their kinetics and the reactant fluxes. Hence, the initial assumption of the hydroxyl group concentration does not affect the results that the model predicts for the growth, once the steady regime is achieved. This however, is valid only if the surface kinetics and the reactant fluxes result in a growth that leads to non full coverage of the surface sites. If the surface kinetics and reactant fluxes allow the deposition process to cover the maximum OH group concentration, the growth is limited by the maximum OH group concentration value. It will be shown below (Fig. 6) that this is the case at 300 °C, where at steady state, the initial OH coverage is close to unity.

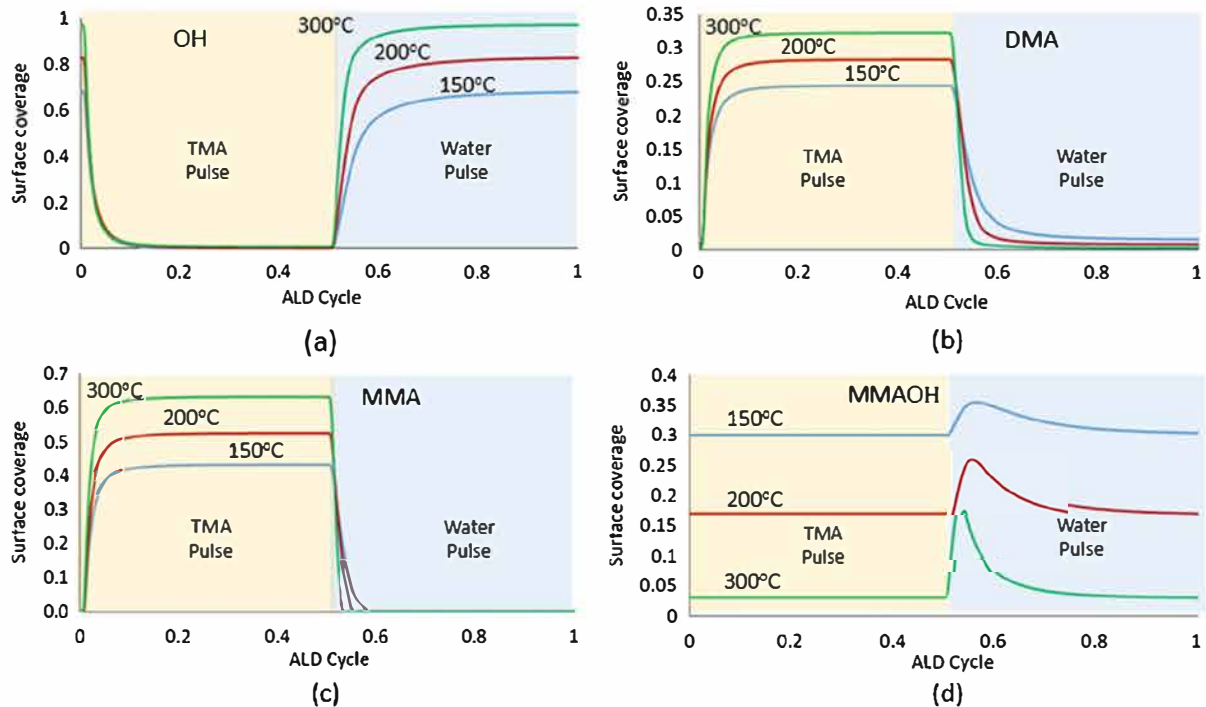


Fig. 6. Model predictions of the surface coverage evolution of the four stable surface species during an ALD cycle, for three different temperatures: (a) OH species coverage, (b) DMA species coverage, (c) MMA species coverage, (d) MMAOH species coverage.

In order to analyze the effect of temperature on the surface kinetics, the surface coverage evolution of the four stable species (OH, DMA, MMA, MMAOH) is presented in Fig. 6 as a function of the ALD cycle. The surface coverages shown are the ones obtained at the center of the wafer once the steady regime has been reached, using a 25 ms TMA pulse. The purge times are not shown. As in Fig. 5, each reactant exposure is equivalent to a half cycle, which equals 1.2 s, for all temperatures, for comparison.

The initial coverage of the OH species during an ALD cycle in the steady state regime increases with temperature, namely 68.5%, 82.6% and 96.8% at 150 °C, 200 °C and 300 °C, respectively. It is worth recalling that, at the steady state regime the species distribution on the surface is regenerated at the end of each cycle. The DMA, MMA, MMAOH species present at the start of each cycle in Fig. 6, are the sum of the species that could not be removed during the TMA and H₂O pulses of the previous non steady regime simulated cycles.

During the TMA pulse, TMA molecules adsorb on the OH surface groups, and react according to reactions (R3) and (R4). So, the OH surface coverage decreases, asymptotically reaching zero. The DMA and MMA species are created, hence leading to the increase of their surface coverage. No significant effect of temperature can be observed on the kinetics of these reactions. This is consistent with results from Vandalon and Kessels (2016, 2017) who showed that the temperature does not have a significant effect on the evolution of the surface methyl group coverage, during the TMA pulse.

The results are different for the H₂O exposure. During the H₂O pulse, water molecules adsorb on DMA and MMA molecules. The H₂O reaction leads to the formation of MMAOH species, on which a second H₂O molecule can adsorb and react. The product of all these surface reactions is the elimination of methyl groups and the formation of OH groups. So, during the H₂O pulse, the OH surface coverage increases and saturates to the initial value of the OH coverage at the start of the ALD cycle. The opposite behavior is observed for the DMA and MMA species, whose surface coverage decreases until they reach their initial value, at the start of the ALD cycle. The MMAOH surface coverage has the behavior of an intermediate species; it is created during the first instants of the H₂O exposure, as a product of the reaction between DMA and adsorbed H₂O species, and then is eliminated, by its reaction with another H₂O molecule. Indeed, its surface coverage first increases, reaching a maximum, and then decreases back to its initial value at the start of the ALD cycle.

The effect of temperature on the evolution of the surface coverage during the H₂O pulse is straightforward. At low temperature, the DMA and MMA group elimination, and then the OH group regeneration are slower. When the temperature is increased, the reactions are faster, explaining that the OH, DMA, MMA groups are regenerated or eliminated faster. The faster reactions of H₂O and DMA species at high temperatures lead to a rapid formation of MMAOH, which reaches its maximum surface coverage faster than in the lower temperature regime (<200 °C). Then the subsequent reaction of MMAOH with H₂O is also favored at higher temperature, leading to the formation of OH groups.

Fig. 6 also shows the mechanisms responsible for the decrease of the GPC at 300 °C. In the steady state regime of the ALD cycle at 300 °C, the initial and final OH surface coverage is 96.9%, which is higher than in the case of 200 °C (82.6%). However, as shown in Fig. 3, the GPC decreases from 200 °C to 300 °C, for the 60 ms TMA pulse. The decrease of GPC at higher temperature is attributed either to the activation of TMA desorption and/or to the decrease of the stable OH groups. Results of Fig. 6 show that the TMA pulse is able to remove almost all the surface OH groups, even for the 25 ms step. Consequently, the major factor limiting the GPC at 300 °C is the maximum number of OH groups that can be present on the surface. This is also validated by the fact that when the TMA

pulse time is increased to 60 ms, the increase of thickness at 300 °C is minimal.

4.2. Growth profile on the substrate

Once validated, it is of main interest to couple the surface kinetic model with the reactor scale CFD one. In our previous fluid dynamic and thermal CFD work, (Gakis et al., 2018) we showed that during the TMA pulse, a recirculation takes place inside the reactor chamber, which results in a non uniform species distribution on the substrate surface. A time snapshot of the flow field and the resulting TMA partial pressure on the substrate surface, for the 300 °C process (simulated experiment 11), is shown in Fig. 7.

Fig. 7 shows that the recirculation taking place in the gas phase above the substrate impacts the species distribution on the substrate, leading to a higher TMA partial pressure on the area between the substrate center and the side of the substrate near the loading door. The recirculation is due to the high speed flow that enters the reactor chamber during the first ms of the TMA pulse.

Fig. 8 shows two alumina thickness profiles obtained in conditions corresponding to experiment 11, performed at 300 °C. The profile in 8a is computed and was obtained by coupling the CFD surface kinetic with model predictions for the GPC profile on the substrate. The profile (8b) is experimental and was obtained through ellipsometry measurements on various points, covering the whole surface of the 200 mm wafer. For better visualizing the experimental measurements, the experimental points are interpolated, and a color map figure was developed in MATLAB®. The two color maps of Fig. 8 have a different color scale, in order to better show the thickness profile shape.

Comparison of the two maps for experiment 11 reveals a qualitative agreement between model predictions and experimental GPC mapping. The higher GPC is obtained between the center of the wafer and the loading door side of the substrate. This GPC profile corresponds to the TMA species distribution profile on the surface, during the TMA pulse, as shown in Fig. 7. We can conclude that the recirculation taking place in the gas phase is dictating the species deposition profile on the substrate surface.

In most cases, ALD is considered as an ideal process, dependent only on surface kinetics. However, the results of Fig. 8, alongside with the results of Fig. 7 and (Gakis et al., 2018) confirm this statement and reveal that the flow field has a direct influence on the GPC profile.

Fig. 9 presents the experimentally determined and computed evolution of the GPC along the surface of the substrate. The results correspond to two process conditions, namely to experiments 11 and 12, characterized by two different TMA pulse durations, 25 ms (experiment 11) and 60 ms (experiment 12). Two different color scales are used: one for the simulation results and one for the experimental measurements.

The measured GPC profile for experiment 11 corresponds to the gas phase TMA species distribution on the substrate, as presented in Fig. 7. When the TMA pulse is increased (experiment 12), a more uniform GPC profile is obtained. The model predictions are in good agreement the experimental measurements.

We set the maximum non uniformity, as the difference between the maximum and the minimum GPC obtained along the substrate, divided by the minimum GPC value:

$$\text{Non uniformity}\% = \frac{\max - \min}{\min} \cdot 100 \quad (17)$$

The experimentally determined maximum non uniformity is 2.40% when using a 25 ms pulse (experiment 11), and decreases to 0.58% for the 60 ms TMA pulse (experiment 12). The equivalent values for the model are 2.45% for the 25 ms (simulation 11) and

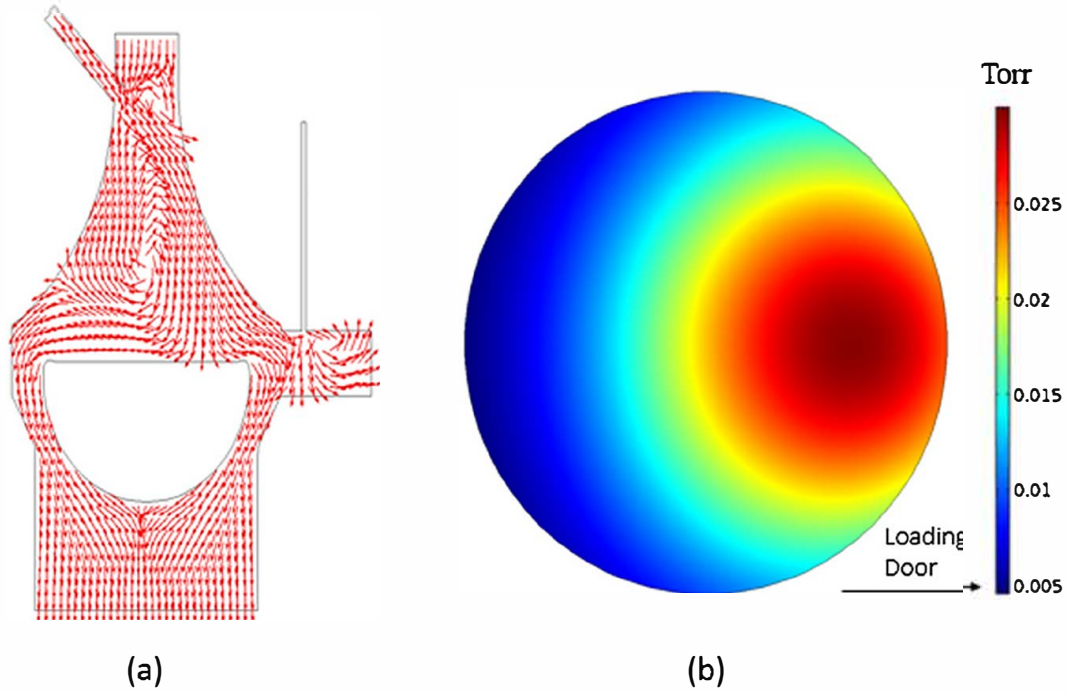


Fig. 7. Snapshots of (a) Flow field inside the reactor, (b) TMA partial pressure on the substrate surface, 25 ms after the start of the TMA pulse, at 300 °C.

0.83% for the 60 ms (simulation 12) TMA pulse. The GPC profile on the surface is also different for the 60 ms TMA pulse. From the above it can be concluded that during experiment 11, the TMA pulse duration was not long enough to allow the adsorption of TMA on the OH groups to eliminate the OH groups on the whole surface. Hence, the recirculation in the gas phase, which dictates the species distribution on the substrate surface, also dictates the thickness profile of the deposited film. In the case of experiment 12, the pulse duration is long enough to cover the OH groups on the whole surface. Hence, the recirculation in the gas phase no longer dictates the thickness profile on the substrate. From the above we can conclude that, in contrast to the preconceived idea

that ALD depends only on surface kinetics, the uniformity of the deposited film can also depend on the process conditions and reactor geometry.

4.3. Effect of purge time decrease

In our previous work, (Gakis et al., 2018) we showed that a low temperature zone was present in the loading door region of the reactor, due to the non heating of the loading door walls. This low temperature zone can seriously affect the purging efficiency, especially for the H₂O exposure. H₂O molecules are more difficult to desorb from cold surfaces. H₂O molecules will adsorb on the

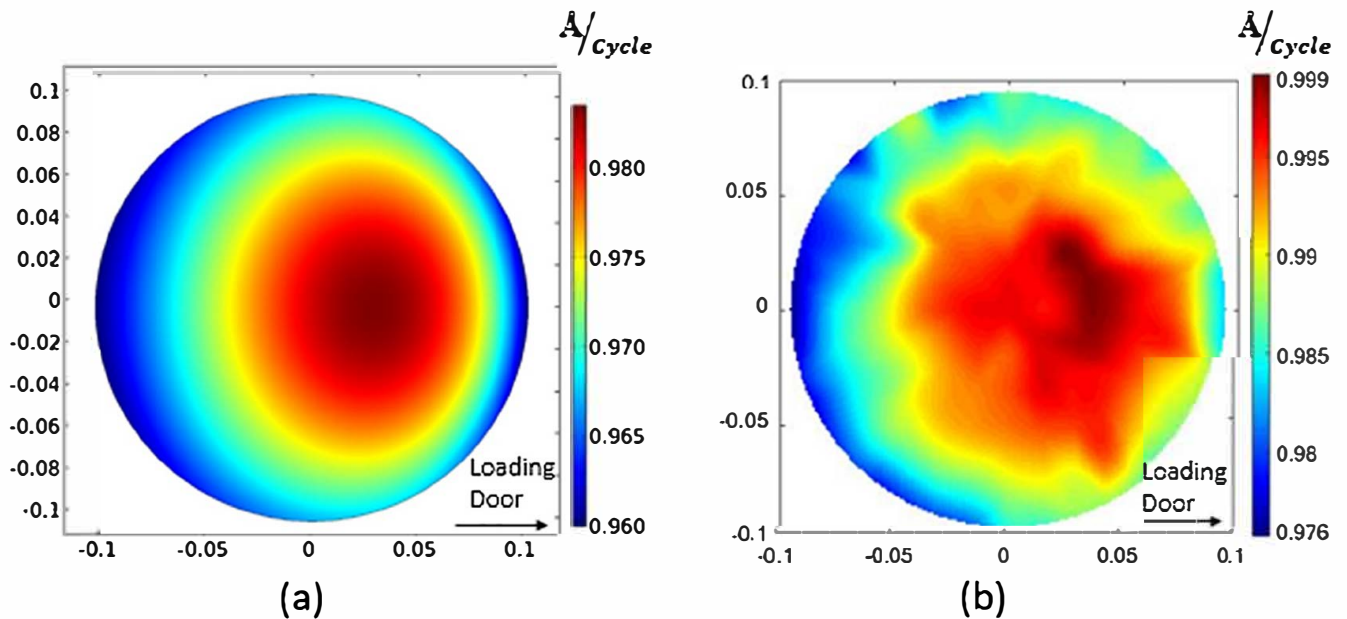


Fig. 8. Profile of the GPC on the substrate surface corresponding to the experiment 11, performed at 300 °C. 8a: Model predictions, 8b: Experimental measurements.

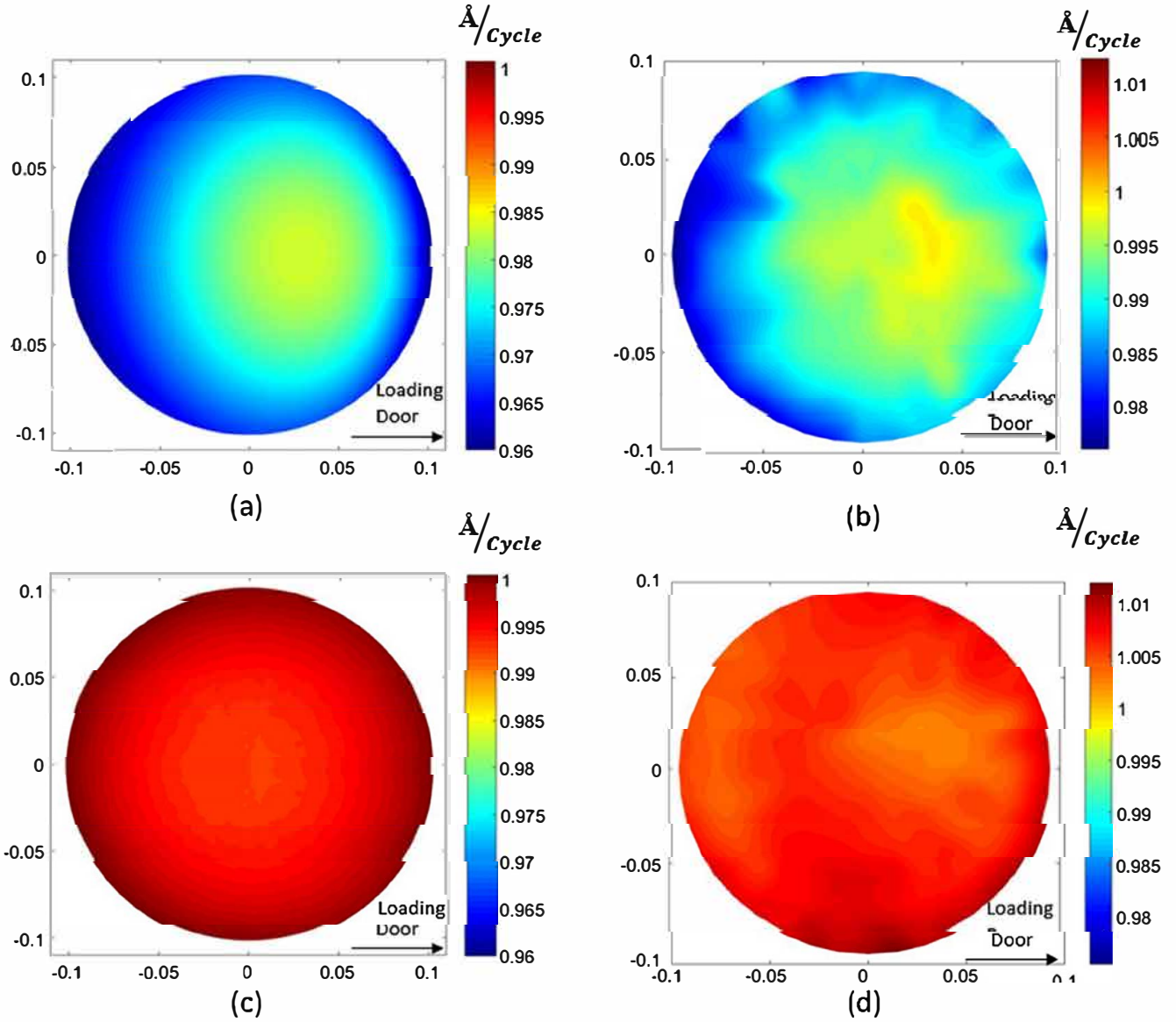


Fig. 9. GPC profile on the substrate surface. (a) Simulated Experiment 11, (b) Experiment 11, (c) Simulated Experiment 12, (d) Experiment 12.

colder loading door walls and will take time to desorb. Hence, this increases the minimum purge time required to remove the reactant species present in the gas phase that could lead to CVD reactions during the next reactant exposure. The CFD model does not take into account CVD reactions and adsorption/desorption on the reactor walls. Hence the purging time effect was studied only by experiments.

In order to see the effect of this low temperature zone on the purging efficiency, a series of experiments using a reduced purge recipe (experiments 13–15 of Table 1) were performed. Thickness of the deposited film was measured along the diameter of the substrate, in order to see the effect of the colder loading door zone on the film uniformity.

The GPC along the substrate diameter is plotted for all four recipes in Fig. 10.

Reducing the purge time in the 300 °C process leads to a significant increase in the GPC all over the substrate surface (experiment 13). This result can be attributed to the occurrence of CVD reactions, due to the co-existence of both TMA and H₂O in the gas phase. The growth profile in the standard purge regime (experiment 11) was found to be dictated by the recirculation in the gas

phase during the TMA pulse, as discussed in Section 4.2. The growth profile is different for the reduced purge regime (experiment 13). Indeed, in experiment 13, a higher GPC is found at the side of the substrate exposed to the loading door. This is attributed to the fact that in the low temperature loading door zone, there is a higher concentration of unremoved species, probably H₂O molecules due to their slow desorption (Chen et al., 1994) from the loading door walls.

At 150 °C, as the temperature is lower, the purge time needs to be increased because the desorption and diffusion processes are slower. When using a standard purge (20 s, experiment 3), the loading door side has a higher GPC than the rest of the substrate. This is caused by the lower temperature close to the loading door for the 150 °C process. The desorption of H₂O molecules being even slower, the 20 s standard purge is not long enough. This effect is also present when the purge time is reduced to 10 s (experiment 14). In this case, the purge time reduction has no effect on the whole side of the substrate that is situated on the opposite side from the loading door. However, on the loading door side of the substrate, the thickness is increased. The closer we get to the loading door, the higher the GPC increase due to purge time reduction.

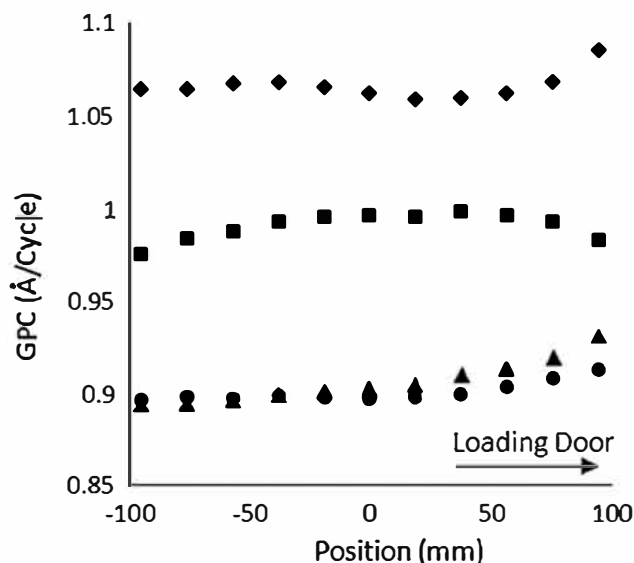


Fig. 10. Effect of the purge time decrease (25 ms TMA pulse). Rhombus: 300 °C reduced purge (experiment 13), Squares: 300 °C 5 s purge (experiment 11), Circles: 150 °C 20 s purge (experiment 3), Triangles: 150 °C 10 s purge (experiment 14).

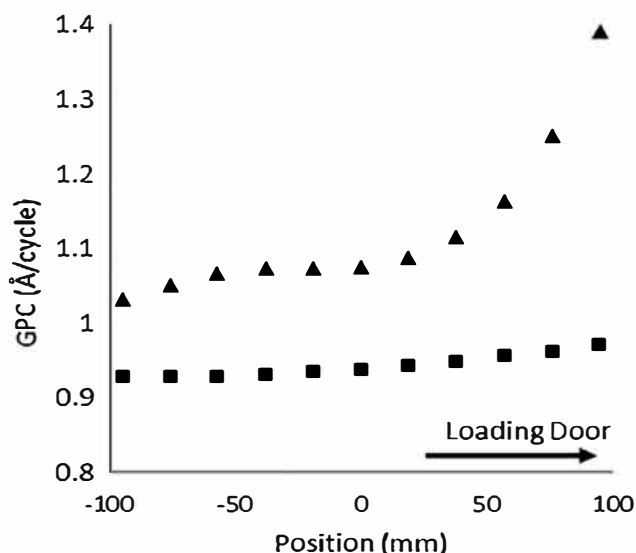


Fig. 11. Effect of the purge time decrease (150 °C, 60 ms TMA pulse). Squares: 20 s purge (experiment 4), Triangles: 5 s purge (experiment 15).

This is expected since the low temperature in the loading door region favors CVD reactions due to unremoved reactants. The maximum non uniformity was 1.8% for the 20 s purge (experiment 3), while this value increased to 4.2% for the 10 s purge (experiment 14). The above results show that a better design of the reactor with a heated loading door would allow the reduction of the purge time to 10 s, ensuring high uniformity, while with the present design even the 20 s purge is not enough to remove the influence of the loading door.

This effect was more evident when the purge time decreased at 150 °C to a highly reduced 5 s purge (experiment 15). The effect of the lower temperature of the loading door zone on the uniformity is shown in Fig. 11, where the GPC profile along the substrate diameter is plotted, for experiments 4 and 15.

The effect of the lower temperature zone in the loading door is clear. For the experiment 4, the GPC is still higher in the loading door side of the substrate, showing that the 20 s purge time is not long enough. The maximum non uniformity is 4.6%, which is higher than for the 25 ms TMA pulse (experiment 3). When the purge is reduced to 5 s (experiment 15), the whole substrate has a higher GPC, proving that CVD reactions take place all over the substrate due to the co existence of reactants in the gas phase. However, the GPC near the loading door is highly increased, leading to a significant increase of non uniformity (maximum value of 34.5%).

5. Conclusions

The chemical surface mechanisms that dictate the growth over the ALD temperature window for Al_2O_3 films deposited using TMA and H_2O vapor were unraveled. To that purpose, ALD experiments were performed in a commercial Ultratech® FIJI F200 ALD reactor on 200 mm silicon wafers; i.e. of industrial interest and large enough to reveal local thickness inhomogeneity, for a variety of process conditions. A complete surface reaction model, coupled to a reactor scale CFD model, (Gakis et al., 2018) which takes into account reactant adsorption, desorption, and surface reactions was developed and validated by comparing the calculated GPC with experimental measurements.

As revealed by an original reaction probability analysis, the competition of surface reactions with desorption is found to be the main factor that limits the growth at low temperature. To the best of our knowledge, the competition between surface reactions and desorption has never been analysed in detail before, for the TMA + H_2O process. The TMA exposure is limited by the adsorption process, and the competition with desorption is not significant. These results are in good agreement with the experimental results of Vandalon and Kessels (2016, 2017) who showed that the H_2O step cannot remove the totality of the surface CH_3 groups, during the H_2O pulse.

Our work also demonstrates that the decrease of the GPC at higher (300 °C) temperature, previously presented in the literature (Ott et al., 1997; Vandalon and Kessels, 2016; Pan et al., 2015; Xie et al., 2015), is mainly due to the decrease of the number of stable surface OH groups present on the surface, which decreases with temperature (Haukka and Root, 1994), and secondarily to the activation of the TMA desorption. It is shown that temperature increase does not significantly impact the TMA kinetics on the surface. However, in the case of H_2O , the time needed for reaching surface saturation was found to decrease with increasing temperature. These results are also in agreement with those of Vandalon and Kessels (2016, 2017).

The effect on the film deposition of the transport phenomena prevailing in the reactor chamber was investigated, both computationally and experimentally. Results show a direct link between phenomena taking place in the gas phase, such as gas recirculation and low temperature zones, and the resulting film uniformity, and thus nuance the established vision of ALD as being solely controlled by surface kinetics. They confirm the necessity to integrate CFD and surface kinetics coupled modelling analyses to the ALD process design and development.

Acknowledgements

This work was partly funded by a Toulouse Tech Inter Lab 2016 grant. GPG acknowledges the financial support by the NTUA Research Committee.

Appendix A. Supplementary material

Supplementary data to this article can be found online at <https://doi.org/10.1016/j.ces.2018.09.037>.

References

- Aria, A.I., Nakanishi, K., Xiao, L., Braeuninger-Weimer, P., Sagade, A.A., Alexander-Webber, J.A., Hofmann, S., 2016. Parameter space of atomic layer deposition of ultrathin oxides on graphene. *ACS Appl. Mater. Interfaces* 8 (44), 30564–30575.
- CHEMKIN-PRO 15131, 2013. Reaction Design: San Diego.
- Chen, J.R., Huang, J.R., Hsiung, G.Y., 1994. Outgassing behavior on aluminum surfaces: water in vacuum systems. *J. Vacuum Sci. Technol. A: Vacuum Surf. Films* 12 (4), 1750–1754.
- Delabie, A., Sioncke, S., Rip, J., Van Elshocht, S., Pourtois, G., Mueller, M., Beckhoff, B., Pierloot, K., 2012. Reaction mechanisms for atomic layer deposition of aluminum oxide on semiconductor substrates. *J. Vacuum Sci. Technol. A: Vacuum Surf. Films* 30 (1), 01A127.
- Dillon, A.C., Ott, A.W., Way, J.D., George, S.M., 1995. Surface chemistry of Al_2O_3 deposition using $\text{Al}(\text{CH}_3)_3$ and H_2O in a binary reaction sequence. *Surf. Sci.* 322 (1–3), 230–242.
- Elam, J.W., Groner, M.D., George, S.M., 2002. Viscous flow reactor with quartz crystal microbalance for thin film growth by atomic layer deposition. *Rev. Sci. Instrum.* 73 (8), 2981.
- Gakis, G.P., Vergnes, H., Scheid, E., Vahlas, C., Caussat, B., Boudouvis, A.G., 2018. Computational Fluid dynamics simulation of the ALD of alumina from TMA and H_2O in a commercial reactor. *Chem. Eng. Res. Des.* 132, 795–811.
- George, S.M., 2010. Atomic layer deposition: an overview. *Chem. Rev.* 110 (1), 111–131.
- Groner, M.D., Fabreguette, F.H., Elam, J.W., George, S.M., 2004. Low-temperature Al_2O_3 atomic layer deposition. *Chem. Mater.* 16 (4), 639–645.
- Haukka, S., Root, A., 1994. The reaction of hexamethyldisilazane and subsequent oxidation of trimethylsilyl groups on silica studied by solid-state NMR and FTIR. *J. Phys. Chem.* 98 (6), 1695–1703.
- Holmqvist, A., Törndahl, T., Stenström, S., 2012. A model-based methodology for the analysis and design of atomic layer deposition processes – part I: mechanistic modelling of continuous flow reactors. *Chem. Eng. Sci.* 81, 260–272.
- Holmqvist, A., Törndahl, T., Stenström, S., 2013a. A model-based methodology for the analysis and design of atomic layer deposition processes – part II: experimental validation and mechanistic analysis. *Chem. Eng. Sci.* 94, 316–329.
- Holmqvist, A., Törndahl, T., Stenström, S., 2013b. A model-based methodology for the analysis and design of atomic layer deposition processes – part III: constrained multi-objective optimization. *Chem. Eng. Sci.* 96, 71–86.
- Holmqvist, A., Magnusson, F., Stenström, S., 2014. Scale-up analysis of continuous cross-flow atomic layer deposition reactor designs. *Chem. Eng. Sci.* 117, 301–317.
- Holmqvist, A., Törndahl, T., Magnusson, F., Zimmermann, U., Stenström, S., 2014. Dynamic parameter estimation of atomic layer deposition kinetics applied to in situ quartz crystal microbalance diagnostics. *Chem. Eng. Sci.* 111, 15–33.
- Johnson, R.W., Hultqvist, A., Bent, S.F., 2014. A brief review of atomic layer deposition: from fundamentals to applications. *Mater. Today* 17 (5), 236–246.
- Jur, J.S., Parsons, G.N., 2011. Atomic layer deposition of Al_2O_3 and ZnO at atmospheric pressure in a flow tube reactor. *ACS Appl. Mater. Interfaces* 3 (2), 299–308.
- Murray, C., Elliott, S.D., 2013. Density functional theory predictions of the composition of atomic layer deposition-grown ternary oxides. *ACS Appl. Mater. Interfaces* 5 (9), 3704–3715.
- Ott, A.W., Klaus, J.W., Johnson, J.M., George, S.M., 1997. Al_2O_3 thin film growth on Si (100) using binary reaction sequence chemistry. *Thin Solid Films* 292 (1–2), 135–144.
- Pan, D., Ma, L., Xie, Y., Jen, T.C., Yuan, C., 2015. On the physical and chemical details of alumina atomic layer deposition: a combined experimental and numerical approach. *J. Vacuum Sci. Technol. A: Vacuum Surf. Films* 33 (2), 021511.
- Peltonen, P., Vuorinen, V., Marin, G., Karttunen, A.J., Karppinen, M., 2018. Numerical study on the fluid dynamical aspects of atomic layer deposition process. *J. Vacuum Sci. Technol. A: Vacuum Surf. Films* 36, (2) 021516.
- Puurunen, R.L., 2005. Correlation between the growth-per-cycle and the surface hydroxyl group concentration in the atomic layer deposition of aluminum oxide from trimethylaluminum and water. *Appl. Surf. Sci.* 245 (1–4), 6–10.
- Puurunen, R.L., 2005. Surface chemistry of atomic layer deposition: a case study for the trimethylaluminum/water process. *J. Appl. Phys.* 97 (12), 121301.
- Remmers, E.M., Travis, C.D., Adomaitis, R.A., 2015. Reaction factorization for the dynamic analysis of atomic layer deposition kinetics. *Chem. Eng. Sci.* 127, 374–391.
- Shaeri, M.R., Jen, T.-C., Yuan, C.Y., 2014. Improving atomic layer deposition process through reactor scale simulation. *Int. J. Heat Mass Transf.* 78, 1243–1253.
- Travis, C.D., Adomaitis, R.A., 2013. Modeling ALD surface reaction and process dynamics using absolute reaction rate theory. *Chem. Vap. Deposit.* 19 (1–3), 4–14.
- Travis, C.D., Adomaitis, R.A., 2014. Modeling alumina atomic layer deposition reaction kinetics during the trimethylaluminum exposure. *Theor. Chem. Acc.* 133 (1), 3–11.
- Vandalon, V., Kessels, W.M.M., 2016. What is limiting low-temperature atomic layer deposition of Al_2O_3 ? A vibrational sum-frequency generation study. *Appl. Phys. Lett.* 108 (1), 011607.
- Vandalon, V., Kessels, W.M.M., 2017. Revisiting the growth mechanism of atomic layer deposition of Al_2O_3 : a vibrational sum-frequency generation study. *J. Vacuum Sci. Technol. A: Vacuum Surf. Films* 35 (5), 4993597.
- Weckman, T., Laasonen, K., 2015. First principles study of the atomic layer deposition of alumina by TMA- H_2O -process. *PCCP* 17 (26), 17322–17334.
- Widjaja, Y., Musgrave, C.B., 2002. Quantum chemical study of the mechanism of aluminum oxide atomic layer deposition. *Appl. Phys. Lett.* 80 (18), 3304–3306.
- Wind, R.A., George, S.M., 2010. Quartz crystal microbalance studies of Al_2O_3 atomic layer deposition using trimethylaluminum and water at 125 °C. *J. Phys. Chem. A* 114 (3), 1281–1289.
- Xie, Y., Ma, L., Pan, D., Yuan, C., 2015. Mechanistic modeling of atomic layer deposition of alumina process with detailed surface chemical kinetics. *Chem. Eng. J.* 259, 213–220.
- Zhuravlev, L.T., 2000. The surface chemistry of amorphous silica. *Zhuravlev model. Colloids Surf., A* 173 (1–3), 1–38.